*New Energy Materials and Devices*
https://www.sciltp.com/journals/nemd

*Article*

# Preparation and Electrochemical Performance of P2-Type $Na_{0.6}Li_{0.1}CoO_2$ Cathode for Sodium-Ion Batteries

Chang-Lu Zheng [1], Ting-Fa Li [2,*] and Xue-Ping Gao [1,*]

[1] School of Materials Science and Engineering, Nankai University, Tianjin 300350, China
[2] Tianjin B&M Science and Technology Co. Ltd., Tianjin 300384, China
* Correspondence: ltf@bamo-tech.com (T.-F.L.); xpgao@nankai.edu.cn (X.-P.G.)

**How To Cite:** Zheng, C.-L.; Li, T.-F.; Gao, X.-P. Preparation and Electrochemical Performance of P2-Type $Na_{0.6}Li_{0.1}CoO_2$ Cathode for Sodium-Ion Batteries. *New Energy Materials and Devices* **2026**, *1*(1), 1–9.

Received: 8 December 2025
Revised: 7 February 2026
Accepted: 12 February 2026
Published: 26 February 2026

**Abstract:** In sodium-ion batteries, layered oxide cathode materials offer the advantage of high electrochemical specific capacity. Especially, their crystal structure can accommodate $Na^+$ ions with a relatively large radius and provide good diffusion pathways, thereby enabling excellent high-rate performance. Among various oxide cathode materials, P2-type layered transition-metal oxides have emerged as highly promising candidates for sodium-ion batteries due to their high capacity, good rate capability, and stable cycling performance. In this work, P2-type $Na_{0.7}CoO_2$ was successfully prepared using $Na_2CO_3$ and $Co_3O_4$ as raw materials through a simple high-temperature solid-state preparation method. Furthermore, the partial substitution of Na with Li is used here to prepare $Na_{0.6}Li_{0.1}CoO_2$. It is confirmed from XRD analysis that both oxides, before and after Li substitution, have the P2-type layered structure with a hexagonal lattice (space group P63/mmc). A trace amount of the $LiCoO_2$ impurity phase is detected in the Li-substituted sample. It is revealed from electrochemical measurements that the $Na_{0.6}Li_{0.1}CoO_2$ cathode delivers the large discharge capacity of 129.7 mAh $g^{-1}$ at 1C rate, representing a 12.6% increase over the pristine $Na_{0.7}CoO_2$. Meanwhile, $Na_{0.6}Li_{0.1}CoO_2$ also exhibits excellent high-rate discharge capability, retaining the discharge capacity of 93.1 mAh $g^{-1}$ at 20 C rate. In addition, $Na_{0.6}Li_{0.1}CoO_2$ cathode shows good cycling stability, with the good capacity retention of 81.8% after 300 cycles.

**Keywords:** sodium-ion batteries; cathode materials; layered oxides; solid-state preparation; partial Li substitution

## 1. Introduction

Lithium-ion batteries have been widely used in portable electronics, electric vehicles, and energy storage technologies owing to their high energy density and excellent cycling stability [1–3]. However, the limited global lithium reserves have become a critical bottleneck restricting the large-scale deployment of lithium-ion batteries in grid-level energy storage systems, highlighting the urgent need to develop alternative technologies based on the abundant sodium resources [4–6]. Sodium-ion batteries, which utilize Na-ions as charge carriers for energy storage and conversion, share a similar working mechanism with lithium-ion batteries. As compared with lithium-ion batteries, sodium-ion batteries offer advantages in resource abundance and potentially lower material costs, making them highly competitive for large-scale energy storage applications. In particular, sodium-ion batteries with polyanionic cathode materials exhibit promising cycling stability for long life energy storage applications. However, their relatively low energy density of the battery with polyanionic cathode limits their application in electric vehicles and portable electronic devices [7–9].

The cathode material is a key factor that determines the energy density of battery system [10–12]. To date, various types of cathode materials have been extensively investigated for sodium-ion batteries, including

**Copyright:** © 2026 by the authors. This is an open access article under the terms and conditions of the Creative Commons Attribution (CC BY) license (https://creativecommons.org/licenses/by/4.0/).
**Publisher's Note**: Scilight stays neutral with regard to jurisdictional claims in published maps and institutional affiliations.

transition-metal (TM) layered oxides, Prussian blue analogues, and polyanionic compounds [13–15]. Among all the cathode materials, TM layered oxides have attracted considerable attention due to their simple preparation routes, abundant raw material sources, and high specific capacity [16–18]. Currently, the most widely investigated TM layered oxides as cathode materials have the P2-type ($Na_xTMO_2$, $0.6 < x < 0.7$) and O3-type ($Na_xTMO_2$, $x = 1$) structures [19–21]. Herein, the P2-type layered oxides exhibit several advantages, such as high structural stability, wide ion diffusion channels, and excellent high rate discharge capability. In particular, P2-type layered oxides demonstrate better cycling stability than their O3-type layered counterparts [22–24]. Among P2-type layered oxides, $Na_{0.7}CoO_2$ is known for its outstanding electrochemical performance and structural robustness, maintaining its crystal structure even when exposed to humid air [25]. For example, Gao et al. prepared a self-supported $Na_{0.7}CoO_2$ nanosheet arrays via the facile "sodiation and post-calcination" method, which exhibit an initial specific capacity of approximately 110 mAh $g^{-1}$ at 1C rate and around 60 mAh $g^{-1}$ at 15C rate [26]. Li et al. synthesized lamellar P2-$Na_{0.7}CoO_2$ material by hydrothermal method, which can provide a maximum capacity of 110 mAh $g^{-1}$ at a current density of 12.5 mA $g^{-1}$, and 60 mAh $g^{-1}$ at a current density of 1250 mA $g^{-1}$ [27]. Herein, it seems that the initial specific capacity of $Na_{0.7}CoO_2$ cathode is hard to exceed 115 mAh $g^{-1}$ at 1C rate. A critical question, therefore, is how to further enhance its performance, particularly in terms of balancing specific capacity, high-rate capability, and cycling stability.

It is demonstrated from previous studies that elemental substitution is an effective strategy for improving the electrochemical performance of oxide cathode materials. In particular, partial substitution of transition metals by lithium can effectively suppress phase transitions in layered oxides during charge–discharge processes, thereby improving their cycling stability. For example, Xu et al. substituted transition-metal ions in the TM layer of layered oxides with Li and successfully prepared O3-type $NaLi_{0.07}Ni_{0.26}Mn_{0.4}Co_{0.26}O_2$. The Li partial substitution in the TM layer is good to suppress phase transitions for improving the electrochemical cycling performance [28]. In addition, Ding et al. introduced Li into the TM layer to obtain a P2/O3 biphasic $Na_{0.67}Li_{0.15}Ni_{0.18}Mg_{0.02}Mn_{0.8}O_2$ oxide. The as-prepared oxide cathode can deliver a high discharge capacity of 160 mAh $g^{-1}$ at 0.1C rate, and show the good cycling stability [29]. Moreover, Chen et al. prepared a Li-substituted P2-type $Na_{2/3}Li_{0.1}Ni_{0.23}Mn_{0.67}O_2$ layered oxide. The Li-substituted P2-type oxide cathode presents a large initial discharge capacity of 121.5 mAh $g^{-1}$, and maintain a good capacity retention of 79.9% after 100 cycles [30]. It should be noted that lithium can substitute not only transition-metal cations in the TM layer, but also can replace sodium ions in the Na layer. It means that such Li partial substitution at Na sites can not only improve the cycling stability of layered oxide cathodes, but also potentially enhance their specific capacity based on the decrease on oxide formula weight. For example, Wang et al. prepared an O3-type $Na_{0.67}Li_{0.2}Fe_{0.4}Mn_{0.4}O_2$ material, and it is revealed by in-situ XRD technology together with neutron powder diffraction that Li partial substitution at alkali sites is helpful to stabilize the layered structure during electrochemical reactions. Moreover, Li partial substitution is also effective to reduce the energy barrier for Na-hopping, thereby facilitating Na insertion/extraction, and leading to the improved cycling stability and high rate performance [31].

In this work, the P2-type $Na_{0.6}Li_{0.1}CoO_2$ layered oxide is prepared via a high-temperature solid-state method by partially substituting Na with Li. The effects of Li partial substitution on the crystal structure, morphology, and electrochemical properties of the as-prepared oxide are investigated in detail. The results indicate that partial Li partial substitution can effectively suppress unfavorable phase transitions, thereby improving the reversible capacity, cycle stability, and high-rate capability of the cathode.

## 2. Experimental

### *2.1. Material Preparation*

P2-type layered $Na_{0.7}CoO_2$ was prepared via a high-temperature solid-state method. Stoichiometric amounts of $Na_2CO_3$ and $Co_3O_4$ powders were thoroughly ground and homogenized, followed by calcination at 800 °C for 48 h under a pure oxygen atmosphere with a heating rate of 5 °C $min^{-1}$, yielding the P2-type $Na_{0.7}CoO_2$ phase. For the Li-substitute samples, $Li_2CO_3$ was added in stoichiometric amounts to partially replace Na at its crystallographic sites, and layered $Na_{0.6}Li_{0.1}CoO_2$ was prepared using the same procedure. Considering the high volatility of sodium at elevated temperatures, 5 wt% excess $Na_2CO_3$ was added during synthesis to compensate for sodium loss during the high-temperature solid-state reaction.

### *2.2. Structural Characterization*

The crystal structures of the samples were analyzed using X-ray diffraction (XRD, Mini Flex II, Rigaku, Tokyo, Japan) with a Cu Kα radiation source ($\lambda$ = 1.54184 Å). Data were collected over a 2θ range of 10–80° at a scanning rate of 4° $min^{-1}$. The microstructure, morphology, and particle size of the materials were examined using scanning

electron microscope (SEM, JSM-7800F, JEOL, Tokyo, Japan), transmission electron microscope (TEM, JEM-2800, JEOL, Tokyo, Japan) coupled with and energy-dispersive X-ray spectra (EDS). The valence states of the constituent elements were characterized by X-ray photoelectron spectra (XPS, Thermo Scientific ESCALAB 250Xi, Waltham, MA, USA). The elemental composition of the active materials was characterized by inductively coupled plasma optical emission spectroscopy (ICP-OES, Agilent 5110, Santa Clara, CA, USA).

### *2.3. Electrochemical Tests*

The as-prepared cathode material, conductive carbon black (Super P), and polyvinylidene fluoride (PVDF) were mixed with *N*-methyl-2-pyrrolidone (NMP) at a mass ratio of 8:1:1. After magnetic stirring for 4–5 h, a homogeneous slurry was obtained and subsequently coated onto the matte side of an aluminum foil using a 100-μm doctor blade. The coated electrodes were dried in an oven at 110 °C for 12 h and then punched into circular disks with a diameter of 10 mm to serve as the working electrodes. Metallic sodium was used as the counter electrode, GF/D glass fiber as the separator, and the electrolyte consisted of 1 mol $L^{-1}$ $NaClO_4$ dissolved in a 1:1 (*v*/*v*) mixture of ethylene carbonate (EC) and propylene carbonate (PC) with an additional 5 vol% fluoroethylene carbonate (FEC). CR2032 coin cells were assembled in an argon-filled glovebox. The mass loading of the active material was with the value ranging from 2.5 to 3.0 mg $cm^{-2}$.

Galvanostatic charge–discharge tests at various current rates were performed on a LAND battery testing system within the voltage range of 2.0–4.0 V. Electrochemical impedance spectra (EIS) were measured using a Zahner IM6ex workstation over a frequency range of 0.1 Hz to 100 kHz. Cyclic voltammetry (CV) was conducted on a CHI600a electrochemical workstation in the potential range of 2.0–4.0 V (vs. $Na/Na^+$) at the scan rate of 0.1 mV $s^{-1}$.

## 3. Results and Discussion

### *3.1. Material Structural Characteristics*

The crystal structures of the samples were characterized and analyzed using XRD patterns, and the results are shown in Figure 1. As presented in Figure 1a, the diffraction peaks of the $Na_{0.7}CoO_2$ sample match well with those of the hexagonal $Na_{0.71}Co_{0.96}O_2$ standard pattern (PDF#30-1182), indicating that the as-prepared oxide has a P2-type layered structure with a hexagonal lattice (space group P63/mmc). In addition, the sharp diffraction peaks suggest that the sample possesses a good crystallinity. From the magnified XRD pattern in the 2θ range of 15–17° as shown in Figure 1b, no shift is observed in the (002) peak, which corresponds to the c-axis characteristic reflection, implying that the interlayer spacing along the c-axis remains unchanged. Similarly, the (102) peak associated with the transition-metal (TM) layer also shows no observable shift. This is likely due to the smaller ionic radius of Li-ions. When Li-ions are used to substitute Na-ions partially, its relatively small size of Li-ions is insufficient to significantly alter either the TM-layer spacing or the c-axis lattice parameter in the Li-substituted sample. Furthermore, no impurity peaks are detected in the $Na_{0.7}CoO_2$, suggesting that the as-prepared product has the pure phase layered structure. In contrast, several weak diffraction peaks appear at 18.9°, 37.4°, 45.2°, and 59.6° in the $Na_{0.6}Li_{0.1}CoO_2$ sample. It is confirmed after comparison with standard patterns that these peaks correspond to $LiCoO_2$ (PDF#50-0653), indicating that trace amounts of the $LiCoO_2$ impurity phase are formed upon the introduction of $Li_2CO_3$ into the Li-substituted sample. XRD Rietveld refinements were performed on the two samples, and the results are summarized in Table 1. Different from neutron powder diffraction (NPD), the substitution sites for Li are hard to obtain based on normal XRD Rietveld refinements. However, the interlayer spacing of (002) plane of $Na_{0.6}Li_{0.1}CoO_2$ can be obtained as shown in Table 1, which is slightly increased as compared to that of $Na_{0.7}CoO_2$ sample. In general, there are two possible substitution sites for Li in the layered structure of Li-substituted TM oxide for Na-ion batteries, the alkali site substitution of Li with smaller ionic radius could decrease the interlayer distance [31]. From this, it can be inferred that Li substitution could be conducted randomly at Na sites/TM sites.

**Table 1.** XRD refinement results of $Na_{0.7}CoO_2$ and $Na_{0.6}Li_{0.1}CoO_2$ samples.

| Sample | a (Å) | c (Å) | $d_{002}$ (Å) |
|---|---|---|---|
| $Na_{0.7}CoO_2$ | 2.8363 (0.0002) | 10.9070 (0.0008) | 5.4354 |
| $Na_{0.6}Li_{0.1}CoO_2$ | 2.8342 (0.0002) | 10.9293 (0.0009) | 5.4419 |

In order to verify whether the elemental ratios in the samples meet the designed requirements, ICP-OES tests were performed on the two samples. The elemental contents are listed in Table 2, which are consistent almost with the expectations within the margin of error.

**Table 2.** The elemental content of Na, Co, and Li in $Na_{0.7}CoO_2$ and $Na_{0.6}Li_{0.1}CoO_2$ samples.

| Sample | Na | Li | Co | Metal Composition |
|---|---|---|---|---|
| $Na_{0.7}CoO_2$ | 14.36% | 0% | 52.13% | $Na_{0.7054}Co_1$-O |
| $Na_{0.6}Li_{0.1}CoO_2$ | 14.00% | 0.70% | 57.68% | $Na_{0.6216}Li_{0.1035}Co_1$-O |

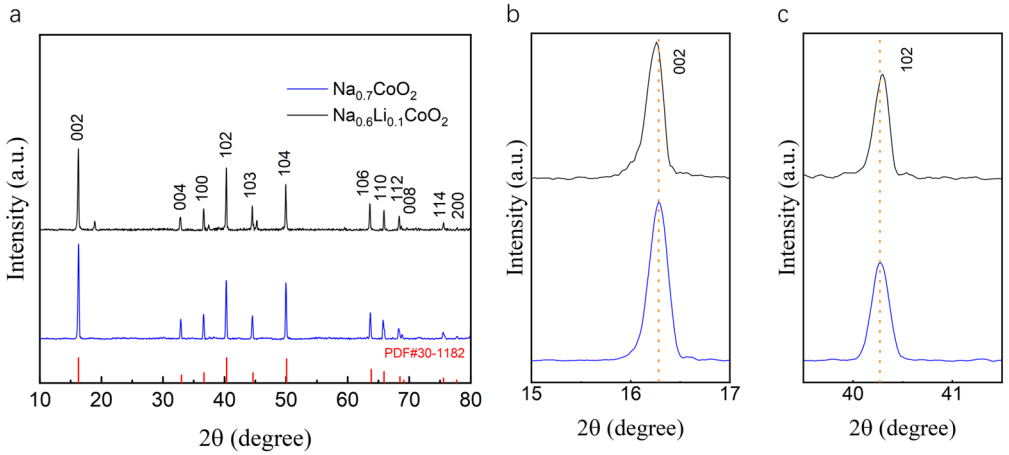


**Figure 1.** XRD patterns of $Na_{0.7}CoO_2$ and $Na_{0.6}Li_{0.1}CoO_2$ samples: (**a**) full patterns; (**b**,**c**) magnified views of selected (002) and (102) peaks.

The morphologies of the samples were examined using scanning electron microscope (SEM), and the images are presented in Figure 2. As shown in Figure 2a, the $Na_{0.7}CoO_2$ sample is consisted of plate-like particles with sharp-edged, quasi-hexagonal shapes and widths of approximately 4–5 μm. The particle surface appears smooth, which is mainly attributed to the strong anisotropy during the crystal growth of layered materials, resulting in step-like surface features due to variations in crystallographic orientations. As seen in Figure 2c, when Li ions are partially introduced into the layered structure, the $Na_{0.6}Li_{0.1}CoO_2$ sample exhibits a significantly rougher and more irregular surface morphology, despite being prepared under identical conditions (calcination temperature and dwell time) to $Na_{0.7}CoO_2$. This surface roughening may be attributed to the altered surface energy caused by partial Li substituting, which disrupts the preferred growth orientation of the layered oxide grains. Additionally, a rougher surface typically corresponds to a higher specific surface area, which increases the interfacial contact between the active material and electrolyte for subsequent electrochemical reaction. It is demonstrated from the elemental mapping results in Figure 2b,d that Na, Co, and O are uniformly distributed in both samples, further confirming the integrity of both the samples. Due to the low atomic number of Li, however, it is difficult to detect Li signals using EDS mapping.

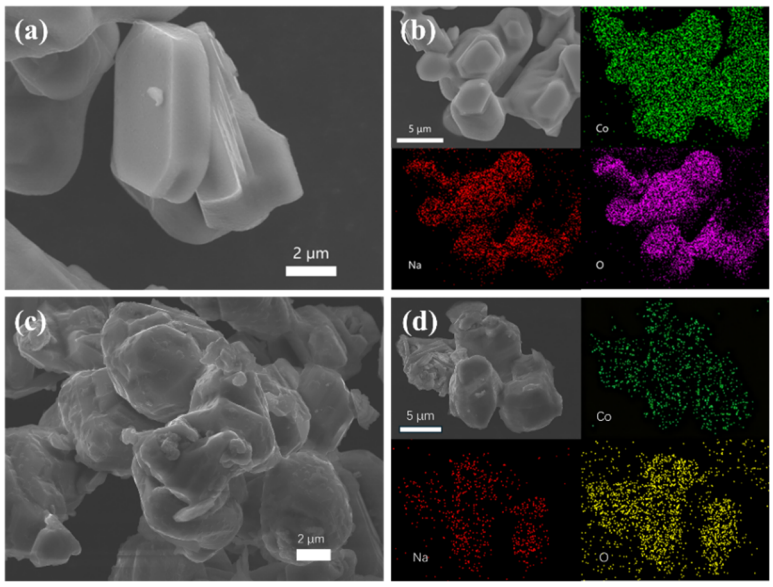


**Figure 2.** SEM images and corresponding EDS-mapping of (**a**,**b**) $Na_{0.7}CoO_2$ and (**c**,**d**) $Na_{0.6}Li_{0.1}CoO_2$ samples.

The microstructures of the samples were further examined using transmission electron microscope (TEM). As shown in Figure 3, both the $Na_{0.7}CoO_2$ and $Na_{0.6}Li_{0.1}CoO_2$ samples exhibit lattice fringes with an interplanar spacing of 0.54 nm based on the TEM measurement accuracy, corresponding to the (002) planes of the layered structure. It indicates that partial substitution of Na by Li does not alter the (002) interlayer spacing in the Li-substituted oxide. The primary reason is that the larger $Na^+$ ions are dominant to support the overall layered framework, while the smaller Li-ions are randomly distributed at Na sites/TM sites and do not alter the layered arrangement. This observation is consistent with the analysis from the XRD patterns in Figure 1.

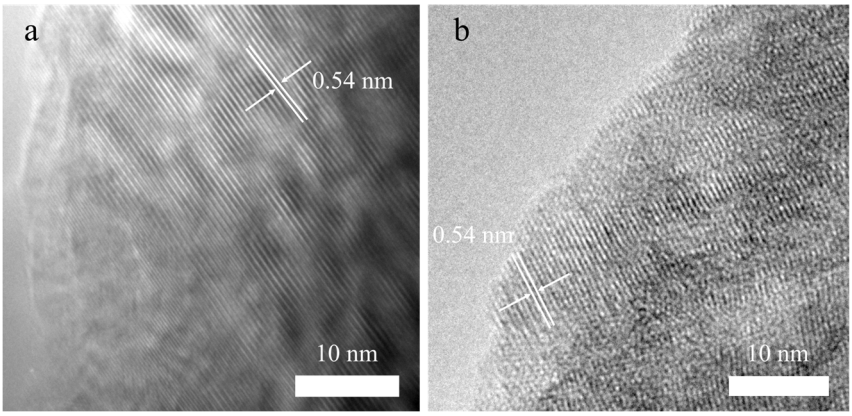


**Figure 3.** TEM images of (**a**) $Na_{0.7}CoO_2$ and (**b**) $Na_{0.6}Li_{0.1}CoO_2$ samples.

The oxidation states of the elements in $Na_{0.7}CoO_2$ and $Na_{0.6}Li_{0.1}CoO_2$ samples were characterized using X-ray photoelectron spectra (XPS), as shown in Figure 4. Due to the low atomic number of Li, the signal of Li-ions in the Li-substituted oxide is hard to be detected by XPS technology. It is confirmed from the survey spectra (Figure 4a,b) that the Na, Co, and O signals are presented in both the samples. In particular, the high-resolution core levels (Figure 4c,d) provide detailed chemical state information for Co. There are four distinct peaks from Co 2p core level: the Co $2p_{3/2}$ peak can be deconvoluted into two components at 779.3 eV and 780.7 eV, while the Co $2p_{1/2}$ peak is fitted with two components at 794.2 eV and 796.1 eV, corresponding to $Co^{3+}$ and $Co^{4+}$, respectively, which is consistent with the characteristics of layered oxides. The peak areas indicate a $Co^{4+}$: $Co^{3+}$ ratio of 1: 0.57 in the oxides. It is shown from comparative analysis that the Co 2p core levels of the two samples are almost identical before and after Li partial substitution, indicating that the partial replacement of Na by Li does not alter the chemical state of Co in the Li-substituted oxide.

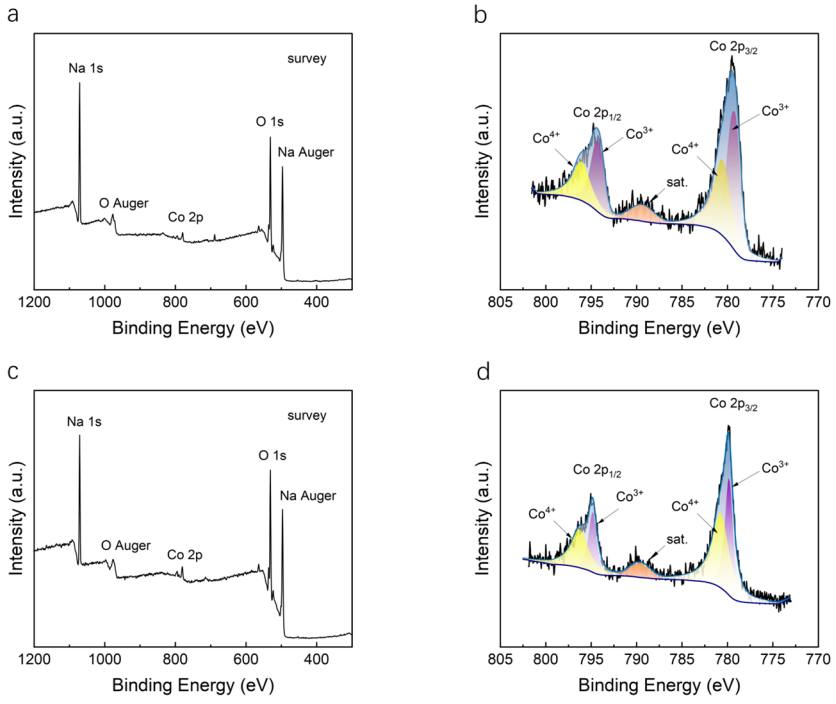


**Figure 4.** XPS spectra of (**a**,**b**) $Na_{0.7}CoO_2$ and (**c**,**d**) $Na_{0.6}Li_{0.1}CoO_2$ samples.

### *3.2. Electrochemical Performance*

To investigate the effect of partial Li substitution for Na on the electrochemical performance of $Na_{0.7}CoO_2$, sodium-ion half-cells were assembled and evaluated, including galvanostatic charge–discharge, high-rate discharge capability, cycling performance, cyclic voltammograms (CVs), and electrochemical impedance spectra (EIS). As shown in the galvanostatic charge–discharge profiles within the 2.0–4.0 V voltage window (Figure 5a), both the cathodes exhibit similar discharge curves and voltage plateaus. Notably, the multiple plateaus at 2.73 V/3.0 V/3.3 V/3.7 V (charging), and at 3.6 V/3.2 V/2.9 V/2.6 V (discharging) can be observed clearly in the charge–discharge profiles, respectively, reflecting the complex phase transitions during insertion/extraction processes of Na-ions. These multiple plateaus can be attributed to the ordering of $Na^+$/vacancies and the sliding of $MO_2$ layers in the insertion/extraction processes of Na-ions [24]. Figure 5b presents the CVs of both the electrodes at the scan rate of 0.1 mV $s^{-1}$. The nearly overlapping CVs indicate that the fundamental electrochemical processes are similar for both the electrodes. Moreover, the multiple redox peaks can be observed in CVs, which is corresponding well with the multi-plateau features in the charge–discharge profiles. As shown in Figure 5c, the $Na_{0.6}Li_{0.1}CoO_2$ cathode exhibits the excellent high-rate discharge capability. More specifically, the $Na_{0.6}Li_{0.1}CoO_2$ cathode can deliver the high specific capacity of nearly 140 mAh $g^{-1}$ at 0.1C rate, and the discharge capacity of 115 mAh $g^{-1}$ at 5C rate. In particular, the cathode still retains over the discharge capacity of 90 mAh $g^{-1}$ at an ultrahigh rate of 20C rate. In comparison, the pristine $Na_{0.7}CoO_2$ cathode can also deliver high discharge capacities at low rates (<2C rate), but shows a pronounced capacity drop at high rates (especially at 10C and 20C rate). Notably, when the discharge current density is restored to 1C rate, the discharge capacity of the $Na_{0.6}Li_{0.1}CoO_2$ is recovered to 130 mAh $g^{-1}$, demonstrating its excellent adaptability to various rate changes.

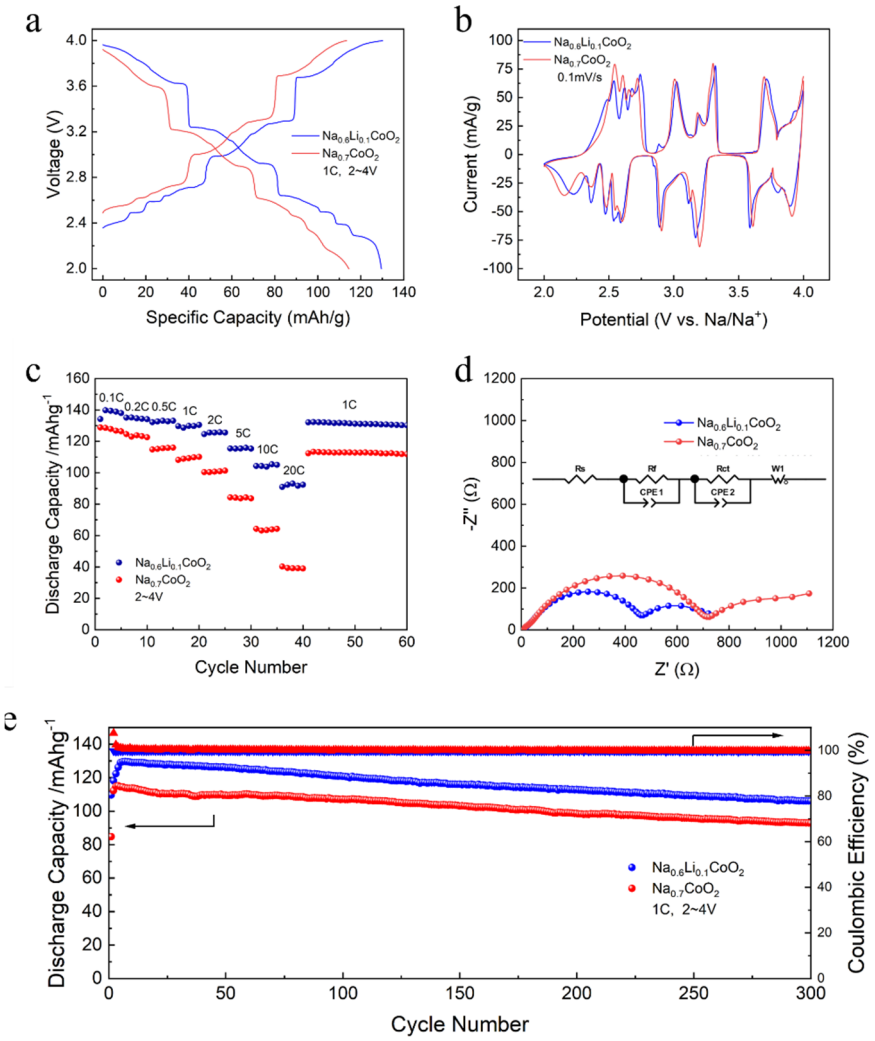


**Figure 5.** Electrochemical performance of $Na_{0.7}CoO_2$ and $Na_{0.6}Li_{0.1}CoO_2$: (**a**) galvanostatic charge–discharge profiles at 1C rate; (**b**) cyclic voltammograms (CVs) at the scan rate of 0.1 mV $s^{-1}$; (**c**) high-rate discharge capability; (**d**) electrochemical impedance spectra (EIS) after 10 cycles; (**e**) cycling performance and coulombic efficiency over 300 cycles.

To further investigate the effect of partial Li substitution on the electrochemical performance, EIS measurements were also conducted on cathodes after 10 cycles (Figure 5d). Both EIS spectra are consisted of two semicircles, corresponding to the formation of solid electrolyte interfacial (SEI) film and surface charge-transfer processes. The EIS fitting results are presented in Table 3, with the equivalent circuit inside Figure 5d [32]. The electrolyte resistances ($R_s$) are smaller for two cathodes, which can be negligible in the impedance analysis. Obviously, both the interface film resistance ($R_f$) and surface charge-transfer resistance ($R_{ct}$) of $Na_{0.6}Li_{0.1}CoO_2$ cathode are smaller than those of $Na_{0.7}CoO_2$ cathode. In particular, the total impedance of the $Na_{0.6}Li_{0.1}CoO_2$ cathode is smaller, indicating that Li substitution can reduce electrode impedance to certain extent, which is beneficial for enhance the high-rate discharge capability of the cathode. Figure 5e shows the cycling performance of the cathodes at 1C rate (1C = 130 mAh $g^{-1}$) within 2.0–4.0 V. Obviously, in the initial 3–5 cycles, the discharge capacities of both cathodes are increased slightly, followed by a gradual decline with further cycling. This initial increase on the discharge capacity is attributed to the incomplete wetting of the cathode by the electrolyte in freshly assembled cells, and the cathodes are activated gradually and stabilized with cycling at the initial stage. In particular, $Na_{0.6}Li_{0.1}CoO_2$ cathode delivers the high initial capacity of 129.7 mAh $g^{-1}$ and retains the discharge capacity of 106.1 mAh $g^{-1}$ after 300 cycles at 1C rate, corresponding to the good capacity retention of 81.8%. In comparison, the $Na_{0.7}CoO_2$ cathode exhibits the low initial capacity of 115.2 mAh $g^{-1}$ and the discharge capacity of 92.9 mAh $g^{-1}$ after 300 cycles, with the capacity retention of 80.6%.

**Table 3.** The EIS fitted data of $Na_{0.7}CoO_2$ and $Na_{0.6}Li_{0.1}CoO_2$ cathodes.

| Cathode | $R_s$/Ω | $R_f$/Ω | $R_{ct}$/Ω |
|---|---|---|---|
| $Na_{0.7}CoO_2$ | 4.27 | 41.39 | 639.8 |
| $Na_{0.6}Li_{0.1}CoO_2$ | 9.20 | 36.21 | 390.3 |

To investigate the morphological changes of the cathode particles after cycling, the cells were disassembled after 300 cycles at 1C rate, and the cathode active materials were examined by SEM (Figure 6). In comparison with the morphologies of the as-prepared oxide samples before cycling as shown in Figure 2, both the samples maintain relatively large grains, with no significant layer delamination, fracture, or pulverization observed after 300 cycles. These results indicate that the as-prepared oxide cathode materials possess good morphological stability during prolonged electrochemical cycling, which is highly important for insuring the stable electrochemical performance of cathode, including the high-rate discharge capability and cycling stability.

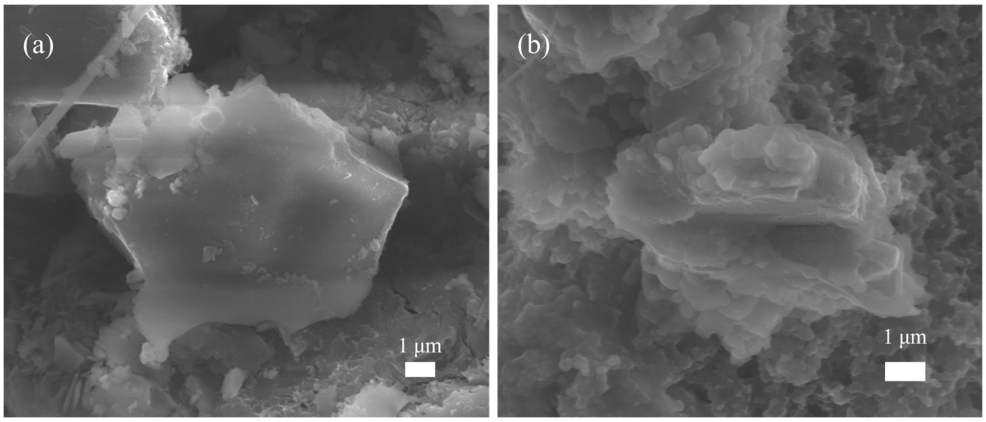


**Figure 6.** SEM images of cathodes after 300 cycles at 1C rate: (**a**) $Na_{0.7}CoO_2$ and (**b**) $Na_{0.6}Li_{0.1}CoO_2$.

## 4. Conclusions

In this work, Li-partially substituted $Na_{0.6}Li_{0.1}CoO_2$ layered oxide cathode materials are prepared via a high-temperature solid-state method. It is demonstrated that, after partial substitution of Na with Li, $Na_{0.6}Li_{0.1}CoO_2$ retains the original P2-type layered structure and similar grain size, while containing trace amounts of a $LiCoO_2$ impurity phase. The introduction of Li modulates the surface energy of $Na_{0.7}CoO_2$, thereby influencing the preferred growth orientation of the grains and altering the microstructure of the particles. This change facilitates the rapid migration of Na-ions in the electrochemical insertion/extraction processes of Na-ions. Li incorporation also suppresses phase transitions during charge-discharge processes of the oxide cathode, helping to preserve the structural integrity and enhance cycling stability while allowing fast extraction of Na-ions. It is shown from electrochemical measurements that the $Na_{0.6}Li_{0.1}CoO_2$ oxide cathode delivers the high initial specific capacity of

129.7 mAh $g^{-1}$ at 1C rate and retains the discharge capacity of 106.1 mAh $g^{-1}$ after 300 cycles, corresponding to the good capacity retention of 81.8%. Additionally, Li partial substitution reduces the electrode impedance to a certain extent, thereby improving the high-rate discharge capability of the cathode. Even at an ultrahigh rate of 20C rate, the as-prepared oxide cathode still delivers the large discharge capacity of 93.1 mAh $g^{-1}$. It means that partial substitution of Na with Li can significantly enhance the specific capacity, cycling stability, and rate performance of P2-type layered oxides, which is promising for the further development of P2-type layered cathode materials.

## Author Contributions

C.-L.Z.: methodology, experiment, data curation, writing-original draft preparation; T.-F.L.: conceptualization, writing—reviewing and editing, funding acquisition; X.-P.G.: supervision, conceptualization, writing—reviewing and editing, funding acquisition. All authors have read and agreed to the published version of the manuscript.

## Funding

This work was supported by the National Natural Science Foundation of China (U24A20500).

## Institutional Review Board Statement

Not applicable.

## Informed Consent Statement

Not applicable.

## Data Availability Statement

Date will be made available on request.

## Conflicts of Interest

The authors declare no conflict of interest. Given the role as Editor-in-Chief, Xue-Ping Gao had no involvement in the peer review of this paper and had no access to information regarding its peer-review process. Full responsibility for the editorial process of this paper was delegated to another editor of the journal.

## Use of AI and AI-Assisted Technologies

During the preparation of this manuscript, the authors used DeepSeek to assist in translating the original Chinese draft into English. The authors subsequently reviewed and edited the translated text as necessary and take full responsibility for the accuracy and integrity of the final content.

## References

1. Chen, S.; Jeong, S.R.; Tao, S. Key materials and future perspective for aqueous rechargeable lithium-ion batteries. *Mater. Rep. Energy* **2022**, *2*, 100096.
2. Zhao, Y.; Kang, Y.; Wozny, J.; et al. Recycling of sodium-ion batteries. *Nat. Rev. Mater.* **2023**, *8*, 623–634.
3. Yang, Y.; Gao, C.; Luo, T.; et al. Unlocking the Potential of Li-Rich Mn-Based Oxides for High-Rate Rechargeable Lithium-Ion Batteries. *Adv. Mater.* **2023**, *35*, 2307138.
4. Thi Thu Hoa, N.; Van Ky, N.; Trung Son, L.; et al. Facile synthesis of cobalt-doped sodium lithium manganese oxide with superior rate capability and excellent cycling performance for sodium-ion battery. *J. Electroanal. Chem.* **2023**, *929*, 117129.
5. Usiskin, R.; Lu, Y.; Popovic, J.; et al. Fundamentals, status and promise of sodium-based batteries. *Nat. Rev. Mater.* **2021**, *6*, 1020–1035.
6. Huang, Z.-X.; Zhang, X.-L.; Zhao, X.-X.; et al. Suppressing oxygen redox in layered oxide cathode of sodium-ion batteries with ribbon superstructure and solid-solution behavior. *J. Mater. Sci. Technol.* **2023**, *160*, 9–17.
7. Song, T.; Chen, L.; Gastol, D.; et al. High-Voltage Stabilization of O3-Type Layered Oxide for Sodium-Ion Batteries by Simultaneous Tin Dual Modification. *Chem. Mater.* **2022**, *34*, 4153–4165.
8. Wang, Y.; Zhao, X.; Jin, J.; et al. Boosting the Reversibility and Kinetics of Anionic Redox Chemistry in Sodium-Ion Oxide Cathodes via Reductive Coupling Mechanism. *J. Am. Chem. Soc.* **2023**, *145*, 22708–22719.
9. Jia, X.-B.; Wang, J.; Liu, Y.-F.; et al. Facilitating Layered Oxide Cathodes Based on Orbital Hybridization for Sodium-Ion Batteries: Marvelous Air Stability, Controllable High Voltage, and Anion Redox Chemistry. *Adv. Mater.* **2024**, *36*, 2307938.

10. Hounjet, L.J. Comparing lithium- and sodium-ion batteries for their applicability within energy storage systems. *Energy Storage* **2022**, *4*, e309.
11. Duffner, F.; Kronemeyer, N.; Tübke, J.; et al. Post-lithium-ion battery cell production and its compatibility with lithium-ion cell production infrastructure. *Nat. Energy* **2021**, *6*, 123–134.
12. Zheng, W.; Liang, G.; Liu, Q.; et al. The promise of high-entropy materials for high-performance rechargeable Li-ion and Na-ion batteries. *Joule* **2023**, *7*, 2732–2748.
13. Peng, B.; Sun, Z.; Jiao, S.; et al. Facile self-templated synthesis of P2-type $Na_{0.7}CoO_2$ microsheets as a long-term cathode for high-energy sodium-ion batteries. *J. Mater. Chem. A* **2019**, *7*, 13922–13927.
14. He, M.; Davis, R.; Chartouni, D.; et al. Assessment of the first commercial Prussian blue based sodium-ion battery. *J. Power Sources* **2022**, *548*, 232036.
15. Gu, Z.Y.; Zhao, X.X.; Li, K.; et al. Homeostatic Solid Solution Reaction in Phosphate Cathode: Breaking High-Voltage Barrier to Achieve High Energy Density and Long Life of Sodium-Ion Batteries. *Adv. Mater.* **2024**, *36*, 2400690.
16. Ouyang, B.; Chen, T.; Liu, X.; et al. Double sites doping local chemistry Adjustment: A Multiple-Layer oriented P2-Type cathode with Long-life and Water/Air stability for sodium ion batteries. *Chem. Eng. J.* **2023**, *458*, 141384.
17. Liu, Y.-F.; Han, K.; Peng, D.-N.; et al. Layered oxide cathodes for sodium-ion batteries: From air stability, interface chemistry to phase transition. *InfoMat* **2023**, *5*, e12422.
18. Wang, X.; Luo, J.; Dou, W.; et al. Stimulating the redox capacity by multi-ion substitution for P2-type sodium-ion battery cathodes. *Mater. Today Energy* **2024**, *43*, 101584.
19. Zhou, D.; Zeng, C.; Ling, D.; et al. Sustainable alternative cathodes of sodium-ion batteries using hybrid P2/O3 phase $Na_{0.67}Fe_{0.5}Mn_{0.5-x}Mg_xO_2$. *J. Alloys Compd.* **2023**, *931*, 167567.
20. Feng, J.; Luo, S.H.; Qian, L.; et al. Properties of the "Z"-Phase in Mn-Rich P2-$Na_{0.67}Ni_{0.1}Mn_{0.8}Fe_{0.1}O_2$ as Sodium-Ion-Battery Cathodes. *Small* **2023**, *19*, 2208005.
21. Shi, S.; Yang, B.; Bai, S.; et al. Ti-doped $O_3$-$NaNi_{0.5}Mn_{0.5}O_2$ as high-performance cathode materials for sodium-ion batteries. *Solid State Ion.* **2024**, *411*, 116554.
22. Pei, Q.; Lu, M.; Liu, Z.; et al. Improving the $Na_{0.67}Ni_{0.33}Mn_{0.67}O_2$ Cathode Material for High-Voltage Cyclability via Ti/Cu Codoping for Sodium-Ion Batteries. *ACS Appl. Energy Mater.* **2022**, *5*, 1953–1962.
23. Hu, H.-Y.; Li, J.-Y.; Liu, Y.-F.; et al. Developing an abnormal high-Na-content P2-type layered oxide cathode with near-zero-strain for high-performance sodium-ion batteries. *Chem. Sci.* **2024**, *15*, 5192–5200.
24. Kang, S.M.; Park, J.-H.; Jin, A.; et al. $Na^+$/Vacancy Disordered P2-$Na_{0.67}Co_{1-x}Ti_xO_2$: High-Energy and High-Power Cathode Materials for Sodium Ion Batteries. *ACS Appl. Mater. Interfaces* **2018**, *10*, 3562–3570.
25. Feng, J.; Fang, D.; Yang, Z.; et al. A novel P2/O3 composite cathode toward synergistic electrochemical optimization for sodium ion batteries. *J. Power Sources* **2023**, *553*, 232292.
26. Gao, L.; Chen, S.; Zhang, L.; et al. Self-supported $Na_{0.7}CoO_2$ nanosheet arrays as cathodes for high performance sodium ion batteries. *J. Power Sources* **2018**, *396*, 379–385.
27. Li, J.; Xiong, S.; Liu, J.; et al. Lamellar P2-$Na_{0.7}CoO_2$ enables long-cycle life of sodium-ion batteries. *Ionics* **2025**, *31*, 10367–10375.
28. Xu, J.; Liu, H.; Meng, Y.S. Exploring Li substituted O3-structured layered oxides $NaLi_xNi_{1/3-x}Mn_{1/3+x}Co_{1/3-x}O_2$ ($x$ = 0.07, 0.13, and 0.2) as promising cathode materials for rechargeable Na batteries. *Electrochem. Commun.* **2015**, *60*, 13–16.
29. Ding, Y.; Wang, S.; Sun, Y.; et al. Layered cathode-$Na_{0.67}Li_{0.15}Ni_{0.18}Mg_{0.02}Mn_{0.8}O_2$ with P2/O3 hybrid phase for high-performance Na-ion batteries. *J. Alloys Compd.* **2023**, *939*, 168780.
30. Chen, Y.; Su, G.; Cheng, X.; et al. Electrochemical performances of P2-$Na_{2/3}Ni_{1/3}Mn_{2/3}O_2$ doped with Li and Mg for high cycle stability. *J. Alloys Compd.* **2021**, *858*, 157717.
31. Wang, J.E.; Han, W.H.; Chang, K.J.; et al. New insight into Na intercalation with Li substitution on alkali site and high performance of O3-type layered cathode material for sodium ion batteries. *J. Mater. Chem. A* **2018**, *6*, 22731–22740.
32. Muruganantham, R.; Chiu, Y.T.; Yang, C.C.; et al. An Efficient Evaluation of F-doped Polyanion Cathode Materials with Long Cycle Life for Na-Ion Batteries Applications. *Sci. Rep.* **2017**, *7*, 14808.